sustainability

Article

Soil Erosion Modelling and Accumulation Using RUSLE and Remote Sensing Techniques: Case Study Wadi Baysh, Kingdom of Saudi Arabia

Nuaman Ejaz [1], Mohamed Elhag [1,2,3,4], Jarbou Bahrawi [1], Lifu Zhang [2], Hamza Farooq Gabriel [5] and Khalil Ur Rahman [6,*]

1 Department of Hydrology and Water Resources Management, Faculty of Meteorology, Environment & Arid Land Agriculture, King Abdulaziz University, Jeddah 21589, Saudi Arabia
2 The State Key Laboratory of Remote Sensing, Aerospace Information Institute, Chinese Academy of Sciences, Beijing 100101, China
3 Department of Geoinformation in Environmental Management, CI-HEAM/Mediterranean Agronomic Institute of Chania, 73100 Chania, Greece
4 Department of Applied Geosciences, Faculty of Science, German University of Technology in Oman, Muscat 1816, Oman
5 NUST Institute of Civil Engineering (NICE), School of Civil and Environmental Engineering (SCEE), National University of Sciences and Technology (NUST), Islamabad 44000, Pakistan
6 State Key Laboratory of Hydro science and Engineering, Department of Hydraulic Engineering, Tsinghua University, Beijing 100084, China
* Correspondence: khalil628@tsinghua.edu.cn

Abstract: This study examines the sediment retention in Wadi Baysh using the Revised Universal Soil Loss Equation (RUSLE) and TerrSet models, accompanied by integrated remote sensing and Geographic Information System (GIS) techniques. The contribution of this study is mainly associated with the application of TerrSet integrated with high resolution datasets to precisely estimate sediments load, which provide useful information to operate dams and improve the operational efficiency of dams. The Advanced Land Observing Satellite (ALOS) Phased Array type L-band Synthetic Aperture Radar (PALSAR) data are utilized to delineate the basin and have been used as an input to the TerrSet model. The rainfall erosivity (R factor) was calculated using the Climate Hazards Center Infrared Precipitation with Stations (CHIRPS) in the research area during 2015–2020. The soil erodibility (K factor) and LULC categorization are calculated using the digital soil map of the world (DSMW) and Sentinel-2 datasets, respectively. The R factor calculated for Wadi Baysh ranges between 91.35 and 115.95 MJ mm/ha/h/year, while the estimated K factor ranges from 0.139 to 0.151 t ha h/ha M. The Support Vector Machine (SVM) method categorized LULC of the study area into four major classes including barren land (81% of the total area), built-up area (11%), vegetation (8%), and water bodies (1%). Results from the sediment retention module (TerrSet) indicated that each year, 57.91 million tons of soil loss occurred in the basin. The data show that soil loss is greater in the northeast and south, whereas it is typical in the middle of Wadi Baysh. It is concluded from the current analyses that the dam lake of Wadi Baysh, located downstream, will be filled soon in the coming few years if sediment loads are carried to the lake at the same rate. Surface dam operators can obtain a full understanding of sedimentation and take proactive measures to reduce its influence on dam operations by leveraging TerrSet's sophisticated capabilities.

Keywords: RUSLE model; CHIRPS; Sentinel-2; GIS application; remote sensing; TerrSet; Wadi Baysh

check for updates

Citation: Ejaz, N.; Elhag, M.; Bahrawi, J.; Zhang, L.; Gabriel, H.F.; Rahman, K.U. Soil Erosion Modelling and Accumulation Using RUSLE and Remote Sensing Techniques: Case Study Wadi Baysh, Kingdom of Saudi Arabia. *Sustainability* **2023**, *15*, 3218. https://doi.org/10.3390/su15043218

Academic Editors: Quoc Bao Pham, Antonietta Varasano and Meriame Mohajane

Received: 17 December 2022
Revised: 4 February 2023
Accepted: 7 February 2023
Published: 9 February 2023

Copyright: © 2023 by the authors. Licensee MDPI, Basel, Switzerland. This article is an open access article distributed under the terms and conditions of the Creative Commons Attribution (CC BY) license (https://creativecommons.org/licenses/by/4.0/).

1. Introduction

Surface dams, including both natural or man-made, are mainly used to store water with other secondary purposes such as power generation and irrigation. However, these reservoirs are threatened by extreme events triggered by climate change and sedimentation by soil degradation in the watershed [1,2]. According to Chuenchum et al. [3], sedimentation affects around 40,000 significant reservoirs globally, resulting in a 0.5% to 1% loss in their storage capacities annually. Further, 80% of the 20 billion tons of sediment that are produced globally are deposited in the oceans each year [4]. Reservoir sedimentation is primarily caused by soil erosion, which occurs naturally but is exacerbated by human activities such as rapid population expansion, deforestation, overgrazing, etc. [5].

Soil erosion is a natural phenomenon that occurs throughout the planet, including in low-sloped areas [6]. Numerous mechanical, biochemical, and microbiological degradations trigger soil erosion. According to Tamene et al. [7], soil erosion is the most serious global environmental issue, resulting in the loss of fertile topsoil, a reduction in soil water-retention capacity, essential vitamins and minerals carried out by the water, dam silting, disruption of aquatic resources, drinking water contamination, and enhanced downstream flooding [8–10]. The loss of fertile soils will exacerbate the fluctuation of food prices and will affect the lives of millions of individuals, potentially pushing them into poverty [11]. However, proper soil management can enhance the food supply, help with carbon storage, and provide means to protect ecosystem functioning [12]. Global soil erosion is accelerated in the twentieth century and is expected to become more severe in some parts of the world in the near future due to extreme climatic changes [13–15]. It is estimated that the average soil erosion globally ranges between 12 to 15 tons per hectare per year [16]. Annually, on average, 0.90–0.95 mm of soil is lost from terrestrial surfaces due to soil erosion [17]. Additionally, more than 75 billion tons of soil is lost yearly due to wind and water erosion [18].

Yeshanesh [19] explained that humans have difficulty while dealing with soil erosion because it is such a complicated phenomenon, and there are so many factors involved in soil erosion such as slope, rainfall, land use, elevation, and vegetation. According to Bahrawi et al. [20], soil erosion is one of the most serious environmental problems in the Kingdom of Saudi Arabia, where soil erosion causes substantial on-site and off-site consequences such as reduced land productivity and sedimentation. The loss of soil from basins can occur in a variety of different ways, each of which can result in both on- and off-site problems. Degradation of the soil and decreased agricultural yield are the two main factors that take place on-site, while the off-site effects include the sedimentation of lakes, dams, and a reduced capacity for storing water [21,22]. Moreover, soil erosion also results in the loss of nutrient-rich topsoil, a deterioration in water quality in places further downstream of the basins, and most importantly, a potential decrease in the capacity of dams and reservoirs to store water, which can lead to a reduction in the efficiency of hydraulic structures [23,24]. The accumulation of sediment in reservoirs throughout the world causes them to lose between 0.5% and 1% of overall storage capability annually. Soil erosion has become an extremely important issue that needs to be resolved through physical and socioeconomic methods [25,26]. In addition to the current status, it is of utmost importance to predict soil erosion and deposition rates for the next few years. Local governments and landowners should make smart decisions to reduce the effects of soil erosion to deal with the current problems and the effects that climate change may have on land use, land cover, and environmental characteristics.

Soil erosion modelling and forecasting have attracted researchers around the globe for more than seven decades [11]; consequently, several models have been developed. The most commonly used models for soil erosion modelling and forecasting include the Soil Erosion Model for Mediterranean Regions (SEMMED) [27], the Water Erosion Prediction Project (WEPP) [28], the Soil and Water Assessment Tool (SWAT) [29], USPED (Unit Stream Power-Based Erosion/Deposition Model) [30], InVEST [31], and TerrSet [32]. The Universal Soil Loss Equation (USLE) and its more recent version, i.e., RUSLE, is the most common model for estimating soil erosion and subsequent sediment deposition in a basin [14,15]. However, the current methods such as the RUSLE and geospatial software programs such as TerrSet give useful information about sedimentation, but they have limitations such as limited geographic reach, inability to monitor in real time, and inability to connect with other tools for managing dams.

The USLE and RUSLE equations are the foundation for several soil loss and sediment delivery models and procedures. The model used in this study is also based on the RUSLE equation. This study will focus on the TerrSet model only, a commercial raster-based package with several modeling capabilities [32]. The primary distinction between TerrSet and other software is that the actual calculation is performed on raster data, but all analyses are conducted on homogeneous surfaces whose parameters are selected when the RUSLE model is initiated and are viewed as isolated patches [6,32]. Many studies show that TerrSet is a good tool for determining the impact of climate change and predicted land use and land cover on soil erosion [6,33,34].

According to the authors' knowledge, no previous research has investigated soil erosion and its deposition with the combined application of TerrSet and RUSLE models in the study area. Moreover, this study also uses rainfall data from CHIRPS to estimate annual precipitation and the R factor that will help to analyze soil erosion with high precision. The contribution of this research to existing literature mainly includes the utilization of the benefits of the TerrSet model, where the RUSLE equation is used as input. This research contributes to improve the operational efficiency of surface dams by utilizing the remote sensing and geospatial data integrated with RUSLE equation and TerrSet model to monitor real-time sedimentation in surface dams. The hydropower generation and water management practices are linked with the water storage capacity of the reservoirs and the sedimentation level, which require precise sediment load estimation. TerrSet allows operators to adapt erosion control and sediment management techniques in real time to ensure dam efficiency and sustainability. Soil erosion is the major problem in the research area; therefore, the aim of this research is given by: (i) the use of remote sensing (RS) and Geographic Information System (GIS) techniques combined with the RUSLE model to map and monitor sediment retention in the TerrSet model, (ii) to provide comprehensive land-use change information using GIS/RS to estimate the annual variations in soil loss, and (iii) application of TerrSet model to improve surface dam operational efficiency by calculating sediment load. Estimating the sediment retention with coupled RS and GIS techniques will help decision and policymakers by pointing out the areas that have been the worst hit and finding high and low-risk areas in terms of soil erosion.

2. Study Area

Wadi Baysh is located in the Jazan region, in the southern part of KSA, and has an area of 4522.81 Km^2. The boundaries of the research area range from longitude 42° 24′ to 43° 27′ E and latitudes 17° 05′ to 18° 03′ N. According to Masoud et al. [35], the study area receives rainfall between 100 and 380 mm yearly, with an average annual rainfall volume of 0.73 to 2.8 billion cubic meters (BCM). The Wadi Baysh is a representative basin of several other basins in the kingdom's southwestern region that are periodically flooded, resulting in damage to infrastructure, loss of soil, and a significant loss of water to the Red Sea [36]. Therefore, a dam was built in the upper section of the Baysh basin to help regulate the flood events. Wadi Baysh is selected as a study region because of its significantly high soil erosion in the area, as well as the influence of sedimentation on water supplies and dam management practices. The semi-arid environment and steep slopes of the Wadi Baysh area make it prone to substantial soil erosion. High levels of soil erosion in the region lead to increased sedimentation in the surface dam, diminishing their storage capacity and efficiency. The prevalence of soil erosion in the Wadi Baysh region presents a unique opportunity to investigate the complexities of the relationship between dam management and sedimentation. The integration of remote sensing techniques with TerrSet model and RUSLE equation in such data-scarce regions will provide opportunities that can be implemented in other similar regions around the globe.

3. Material and Methods

3.1. Data Collection

To carry out this research, we used different types of data given in Table 1. ALOS PALSAR DEM with 12.5 m resolution was acquired in this research from Earth Data from Alaska Satellite Facility (ASF) Data Search Vertex [37]. This DEM is used to extract the basin and stream networks for the study using the Arc Hydro tool in ArcGIS 10.7, as shown in Figure 1c. In addition, this DEM is used as a single parameter for sediment retention in the TerrSet model.

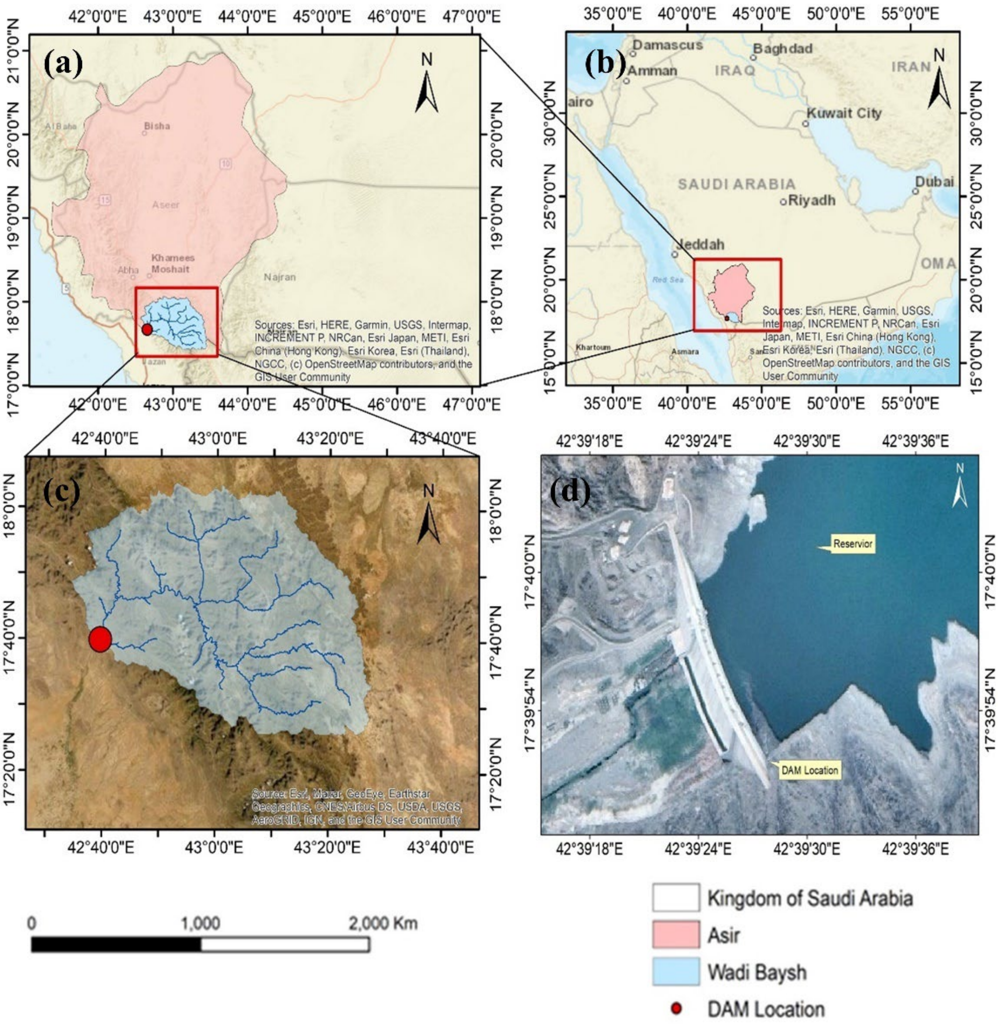

Figure 1. Geographical location of the study area (**a**) Asir Region, (**b**) Wadi Baysh, (**c**) Meteorological stations in Wadi Baysh, (**d**) DAM location in Wadi Baysh.

Table 1. Details of the input datasets used in this study.

Data	Spatial Resolution	Source
Digital Elevation Model (DEM)	12.5 m	ALOS PALSAR
Climate Data	0.05° × 0.05°	CHIRPS Dataset
Soil Data	30 m	DSMW Data
Land Use Land Cover	10 m	Sentinel-2 Data

CHIRPS is a relatively new precipitation data product developed using various data sources and has an excellent spatiotemporal resolution. The USGS, Earth Resources Observation Sciences (EROS), and the Santa Barbara Climate Hazards Group at the University of California collaborated to develop this product [38,39]. CHIRPS integrates 0.05° resolution satellite images with in situ station data to construct gridded rainfall time series over a region spanning 50°S–50°N with all longitudes, beginning in 1981 and continuing to the current day [40]. This work utilizes monthly and annual CHIRPS precipitation data from 1 January 2015 to 31 December 2020 from three stations in the research area (A121, A104, and SA145), as shown in Figure 1d.

To develop the soil map and determine the soil erodibility (K factor), we used the DSMW dataset in the current study due to the unavailability of the other input data. DSMW data can be freely accessed using this link [41]. DSMW soil has a spatial resolution of 30 m. The Sentinel satellites were launched on 23 June 2015, as a part of the Sentinel-2 mission. Two operational satellites are required to attain high mission availability and a 5-day geometric revisit duration [42]. With one operational satellite of Sentinel-2 at the beginning of system deployment, the revisit interval is ten days. Landsat-7 has a geometric revisit length of 16 days, whereas SPOT has a revisit period of 26 days; neither provides systematic land surface coverage [43,44]. Therefore, Senitnel-2 data in the current study are used for the Land Use and Land Cover (LULC) classification. The spatial resolution of the Sentinel-2 ranges from 10 m to 60 m. The data have been downloaded using the United States Geological Survey (USGS) Earth Explorer website.

3.2. TerrSet

TerrSet is a RS and GIS analysis tool created by Clark University's Clark Labs. It features capabilities for image processing, data visualization, and modeling, and its applications include the detection of land-use and land-cover change, the creation of digital elevation models, and the management of natural resources [32]. TerrSet is compatible with numerous raster and vector data formats.

TerrSet provides a sediment retention module for modeling and analyzing sediment retention within a basin [6]. This module contains tools for generating DEMs and determining topographic indices such as flow accumulation and flow direction, which can identify locations with a high propensity for erosion and prioritize management measures such as soil conservation and replanting [45]. In addition, the module has tools for modelling sediment transport and retention using the Universal Soil Loss Equation (USLE) and the Revised Universal Soil Loss Equation (RUSLE) models. Moreover, the module has the capacity to develop maps and charts that can assist decision-makers in visualizing and comprehending the sediment retention issue.

3.3. RUSLE Model

Renard et al. [46] developed the RUSLE equation for basin-scale applications. The fundamental of the RUSLE model is to estimate mean annual soil loss. This analysis method allows us to make maps to fully understand the areas at risk of soil erosion. The RUSLE equation is the foundation for the sediment module in the TerrSet software. The basic equation of RUSLE model is presented as follows:

$$A = R \times K \times LS \times C \times P \quad (1)$$

where the average annual soil erosion rate is denoted by A (ton $h_a{}^{-1} y_r{}^{-1}$); the rainfall erosivity is shown by R (MJ. mm $h_a{}^{-1} h^{-1} y_r{}^{-1}$); soil erodibility is represented by K (ton ha h MJ^{-1} $h_a{}^{-1} mm^{-1}$); LS is the slope length and slope steepness factor (dimensionless); C is the correction coefficient for the effect of vegetation (dimensionless), and P is the correction coefficient used to integrate the effect of soil erosion control measurements (dimensionless). The overall method used in this research is shown schematically in Figure 2. RUSLE is a robust model most commonly used due to its flexibility. The model parameters required for TerrSet are given in the following Table 2.

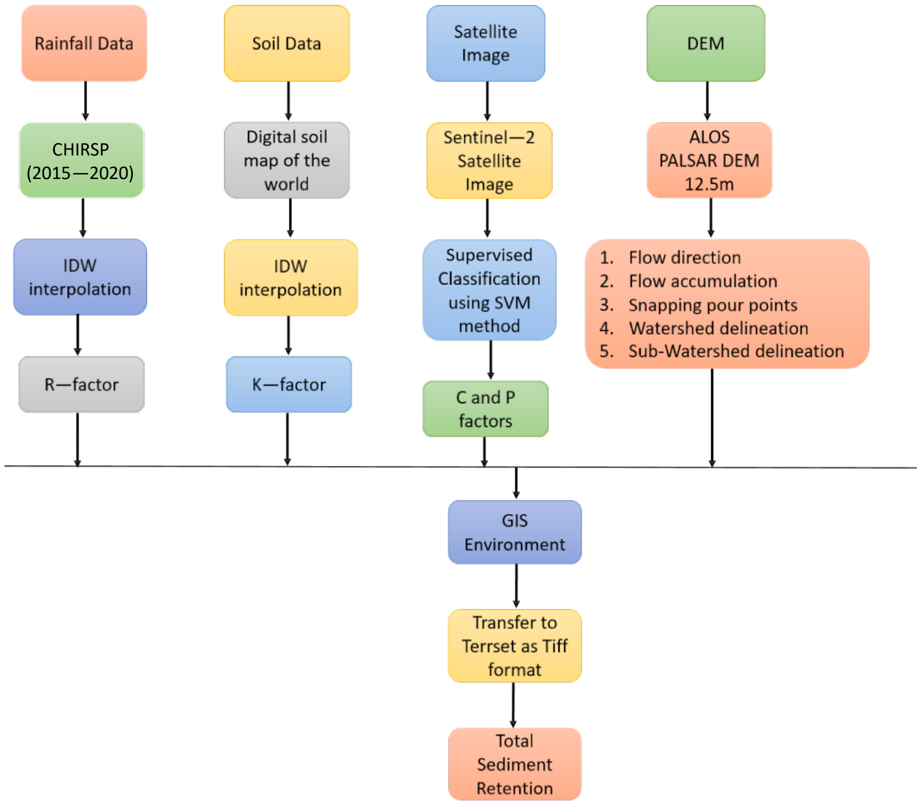

Figure 2. Flowchart showing conceptual framework to determine the sediment retention in TerrSet Model.

Table 2. Information about the basic parameters and their format used in the TerrSet model.

Parameters	Format for Parameter
Watershed	Raster file
Sub Watershed	Raster file
Land Use Land Cover	Raster file
DEM	Raster file
R Factor	Raster file
K Factor	Raster file
Sediment Threshold table	Numerical Value
Bio Physical table	Numerical Value
Geodata format	Idrisi file (.RST)

3.3.1. R Factor

The rainfall erosivity factor (R) and its estimation are largely reliant on yearly rainfall (mm) data; when annual rainfall is high, erosivity (R) is likewise high. The rainfall erosivity factor (R) is the function of average annual rainfall. The spatial distribution of rainfall is created using inverse distance weighting (IDW) in ArcMap. The IDW is one of the most accurate methods while calculating the spatial rainfall distribution [47–49]. According to Hurni [50], the best equation used to calculate R for any arid region is given below:

$$R = -8.12 + 0.562 \times PCP \quad (2)$$

where PCP = annual rainfall (mm/yr^{-1}).

3.3.2. K Factor

To estimate the K factor, we used the Williams equation as suggested by several studies [51–53]. The equation is given below:

$$K_{USLE} = f_{csand} \cdot f_{cl-si} \cdot f_{orgc} \cdot f_{hisand} \quad (3)$$

where f_{csand} (fraction of coarse sand) decreases the K factor values in soils with high coarse sand and increases for soils with little sand; f_{cl-si} (ratio of fraction of clay to silt) reduces K factor values for soils containing a high proportion of clay to silt; f_{orgc} (fraction of organic carbon) reduces K values in soils with a high organic carbon content, while f_{hisand} (fraction of high sand) reduces K values for soils with excessively high sand concentrations.

$$f_{csand} = \left(0.2 + 0.3 \cdot \exp\left[-0.256 \cdot m_s \cdot \left(1 - \frac{m_{silt}}{100}\right)\right]\right) \quad (4)$$

$$f_{cl-si} = \left(\frac{m_{silt}}{m_c + m_{silt}}\right)^{0.3} \quad (5)$$

$$f_{orgc} = \left(1 - \frac{0.25 \cdot orgC}{orgC + \exp[3.72 - 2.95 \cdot orgC]}\right) \quad (6)$$

$$f_{hisand} = \left(1 - \frac{0.7 \cdot \left(1 - \frac{m_s}{100}\right)}{\left(1 - \frac{m_s}{100}\right) + \exp\left[-5.51 + 22.9 \cdot \left(1 - \frac{m_s}{100}\right)\right]}\right) \quad (7)$$

where m_s, m_{silt} , m_c, and orgC denotes the percent of sand content ranges between (0.05–2.00 mm diameter), the percent of silt content from (0.002–0.05 mm diameter), the percent of clay content (<0.002 mm diameter particles), and organic carbon content of the soil layer in percent.

3.3.3. LULC Preparation

The LULC for Wadi Baysh is prepared using Sentinel-2 data, which are processed in ENVI 5.3. All the satellite images are stacked using the stacking tool, and then the pan-sharpening tool is used to increase the image's resolution to 10 m. The training areas are chosen to create hyperplanes that divide the data into different LULC classes. Support Vector Machines (SVM) are great for employing machine learning methods to identify high-dimensional remote sensing data [54,55]. The confusion matrix and kappa coefficient have become common methods for evaluating the correctness of LULC classes [56,57]. In this study, a discrete multivariate technique called Kappa analysis is employed to assess the accuracy for the developed LULC maps [58,59]. The following equation is used to calculate Kappa coefficient [60].

$$Kappa = \frac{N\sum_{i=1}^{r} x_{ii} - \sum_{i=1}^{r}(x_i + \times x_{+i})}{N^2 - \sum_{i=1}^{r}(x_{ii} \times x_{+i})} \quad (8)$$

where r is the number of columns and rows in the error matrix, N represents the total number of pixels, X_{ii} shows the samples in column i and row i, $Xi+$ depicts the marginal total of row i, and $X + i$ denotes the marginal total of column i.

A Kappa coefficient of 1 indicates complete agreement, whereas a number near to zero indicates poor agreement. For overall accuracy, the following Equation (8) is used.

$$\text{Overall accuracy} = \frac{\text{Number of accurate samples}}{\text{Total Number of samples}} \quad (9)$$

Google Earth was used to validate the ground truth samples for each land-use class with LULC's classified pixels at random locations. The erosion risk maps were generated by integrating all pre-estimated factors in Equation (1) to generate an erosion map. These maps were accomplished by using TerrSet and GIS environment.

4. Results

4.1. RUSLE Model Parameters

4.1.1. R Factor

R factor map for Wadi Baysh was created from the mean annual rainfall of the stations using the inverse distance weighted (IDW) method. Figure 3 shows that the mean R factor varied from 91.35 to 115.95 MJ mm/ha/h/year in the study area, with the highest values in the mountainous region and typically low in the steep parts of the basin. The results indicate that the R factor's value is higher in the northern region and lower in the southern region of Wadi Baysh.

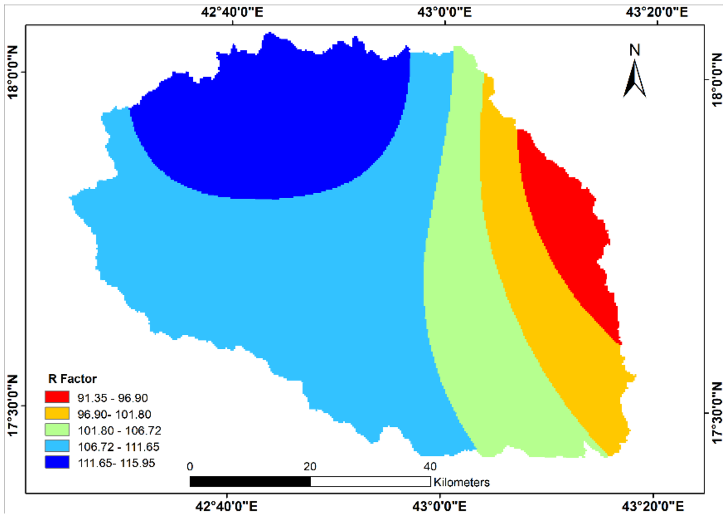

Figure 3. Rainfall erosivity factor map of Wadi Baysh developed using CHIRPS data and IDW spatial distribution technique in ArcGIS.

4.1.2. K Factor

Figure 4 shows the spatial variation of K values in Wadi Baysh, where its values range from 0.139 to 0.151 t ha h/ha M.J. mm, indicating low-to-moderate soil erodibility. The K factor is divided into two classes, i.e., high (green color) and low erodibility (red color). Table 3 shows soil type, soil texture, and K values in Wadi Baysh. The K values are calculated using Equations (3)–(7). The first type of soil class consists of 58.9% sand, 16.2% silt, 24.9% clay, and 0.97% organic carbon. In contrast, the second class is comprised of 75% of sand, 15% silt, 10% clay, and 0.31% organic carbon. Soils with higher K values are more vulnerable to soil erosion. However, lower K values are more resistant to soil erosion.

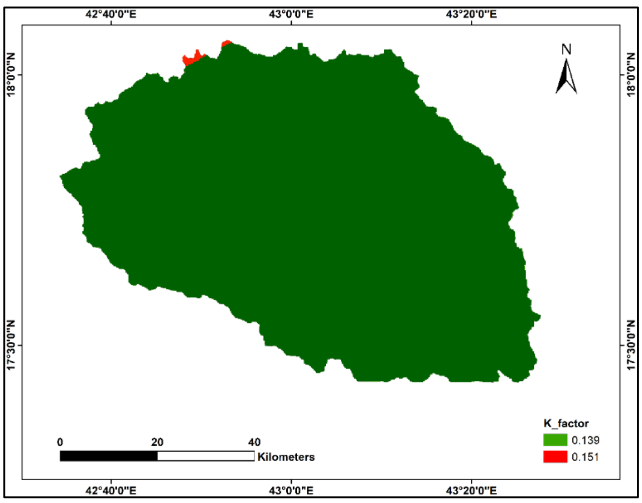

Figure 4. Shows the soil erodibility map of Wadi Baysh.

Table 3. Soil texture, soil type, and their K values.

Soil Unit Symbol	Soil Type	Sand %	Silt %	Clay %	Organic Carbon %	Soil Type	K Factor
I	Lithosols	58.9	16.2	24.9	0.97	Loam	0.139
I	Lithosols	75	15	10	0.31	Loam	0.151

4.1.3. LULC

The Baysh basin is classified into four categories: barren land, built-up water bodies, and vegetation (shown in Figure 5). The finding reveals that 81% of the total area is barren land, 11% is built-up, 8% is vegetation, and 1% is water bodies. Most of the barren land is composed of rocks, stones, and xerophytes. The Kappa coefficient is used to check the accuracy of the classification. The overall accuracy is 86%, while the Kappa coefficient is 0.76 of the classification based on SVM, as shown in Table 4.

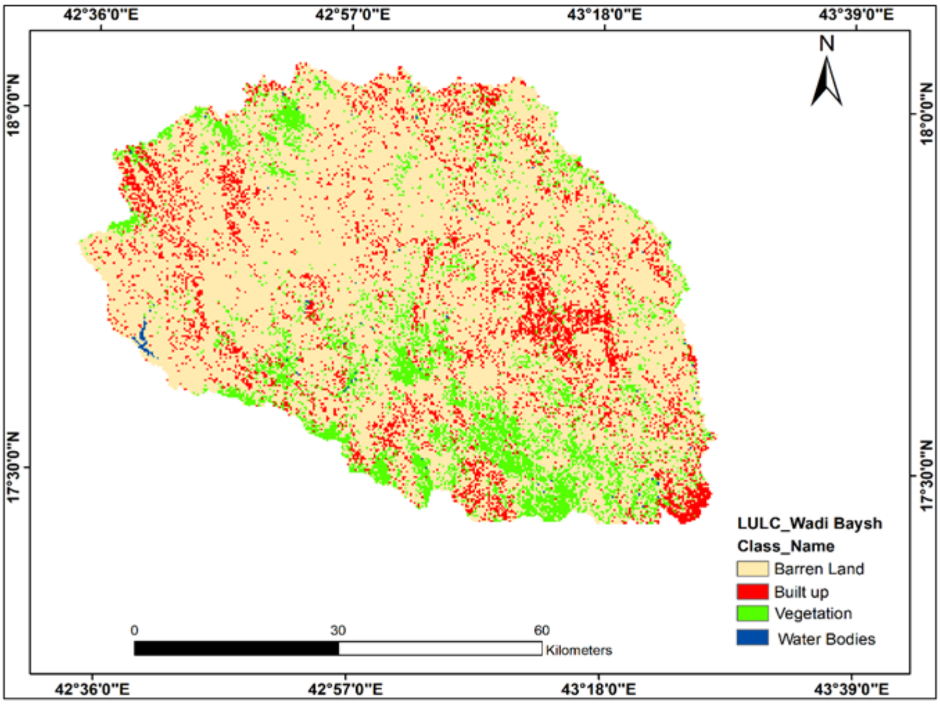

Figure 5. Land Use Land Cover map of Wadi Baysh.

Table 4. Accuracy assessment of Land Use Land Cover based on Kappa Coefficient for Wadi Baysh.

Land Cover	Barren Land	Built Up	Vegetation	Water Bodies	Total	User Accuracy	Commission
Barren Land	50	6	2	1	59	84.75	15.25
Built up	2	13	0	0	15	86.67	13.33
Vegetation	1	1	8	0	10	80.0	20.0
waterbodies	0	0	0	8	8	100.0	0.0
Total	53	20	10	9	92		
Producer Accuracy	94.33	65.0	80.0	88.89			
Omission	5.67	35.0	20.0	11.11			
Kappa	0.76						
Overall Accuracy	86						

4.1.4. Total Estimated Sediment Retention in the Basin

The spatial distribution pattern of annual sediment load (shown in Figure 6) in Wadi Baysh was estimated by adding all the RUSLE parameters into the Sediment retention module inside the TerrSet environment. The total annual soil loss estimated by the TerrSet in the basin is 57.91 million tons, which occurred from an area of 4568.1 km^2. The soil erosion map is classified into three categories (green, yellow, and red) on the basis of erosion risk. The green color shows a very slight and low potential for soil erosion and is dominantly located in the plan and urban area (downstream and middle part) of Wadi Baysh. Similarly, the red color shows the high erosion risk value of the basin (57.91 tons/ha/year) that occurred at the mountain area (upstream) near the Dam of Wadi Baysh, and the yellow color expresses the mild soil erosion potential. According to the findings, the basin is experiencing relatively significant spatial variations in soil loss due to the major differences in topographical conditions, agricultural practices, land-cover changes, and increased rainfall fluctuation.

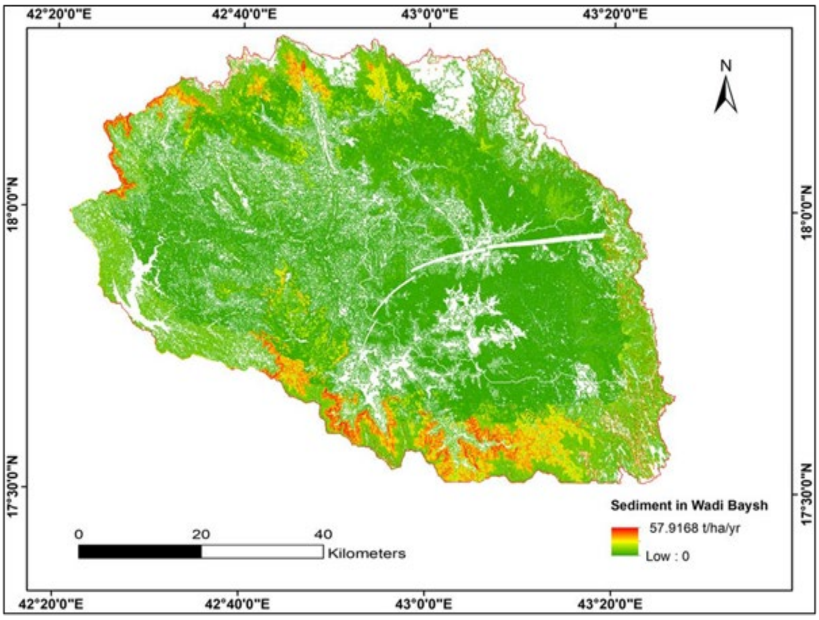

Figure 6. Sediment accumulation in the Wadi Baysh using the TerrSet model.

5. Discussion

In this study, the Baysh basin was delineated using the ALOS PALSAR DEM, and the downloaded DEM was used as input to the TerrSet model. Rainfall data from the CHIRPS satellite are used to calculate the R factor for the study during 2015–2020. Furthermore, the K factor was estimated using the DSMW data, while LULC classification maps were developed using the Sentinel-2 data.

Soil erosion is caused by both natural and human factors [47]. It is necessary to comprehend and estimate the extent and causes of soil erosion, figure out how to stop it. Several models were developed and proposed on a global scale to quantify soil erosion at various spatial scales. RUSLE is a globally accepted, reliable method for calculating soil losses and sediment transport [61,62]. The model effectively estimates soil erosion with limited data in arid regions where data are scarce [63,64]. Erosion is a major issue in various local and regional areas, particularly those with extensive arid and semiarid regions, such as KSA, which are characterized by long dry seasons [65,66]. Rainfall erosivity, soil erodibility, and LULC factors, which are the primary parameters for estimating soil loss in the RUSLE model, contribute to soil erosion [67,68]. Separate spatial maps of RUSLE parameters were prepared for this study and used in TerrSet software to estimate sediment retention.

Our findings show that annual soil loss per year in Wadi Baysh is 57 t ha^{-1} yr^{-1} (Figure 6). This was correlated with similar studies carried out in KSA and different parts of the world. It is analyzed from the comparison that the rates of soil erosion are alike across all regions. Elhag et al. conducted recent research on two arid basins (Yalamlam and Al-Lith) of KSA and found that the annual soil losses ranged from 10 t/ha/year to 40 t/ha/year in both basins. Azaiez et al. [69] used FAO and RUSLE equations to monitor soil loss in Wadi El Hayat in the Jizan region and found the soil loss to be between 36.1 tons/ha/year for

FAO and 40 tons/ha/year for the RUSLE equation. Bahrawi et al. [20] used the RUSLE and RS techniques to assess soil erosion in the Wadi Yalamlam basin southeast of Jeddah, KSA, and calculated annual soil loss of 40 t ha^{-1} yr^{-1}.

The findings of this research are also compared with studies conducted around the world. From the comparison it is clear that the patterns of soil erosion vary by region. For example, the findings in this study show that the average soil erosion rate in Wadi Baysh is higher than the findings of a study conducted by Wolka et al. [70] who reported an average erosion rate of greater than 45 tons/hectare/year in Chaleleka wetland watershed, Central Rift Valley of Ethiopia. On the other hand, the magnitude of soil erosion in Wadi Baysh is lower than the average erosion rate of 78 tons/hectare/year in the Chitral district of Pakistan [61]. Another study conducted by Tirkey et al. [71] reported an average erosion rate of 69 tons/hectare/year in the Daltonganj Watershed of Jharkhand (India). Jazouli et al. [34] estimated the average annual soil loss of 58 t ha^{-1} yr^{-1} in 2003, and the predicted annual soil loss average for 2030 will be 60 t ha^{-1} yr^{-1} in the arid and semi-arid basin of the Oum Er Rbia River (Morocco). In terms of soil degradation, one of the most significant environmental issues that KSA faces is soil erosion [65]. Erosion of the soil results in significant on-site and off-site impacts, such as a significant decrease in the land's productive capacity and sedimentation. These impacts can be attributed to the amount of soil erosion primarily determined by a number of factors, including vegetation cover, terrain, type of soil, and weather [20,65,66].

Dam performance and longevity depend on the sediment load and dam management practices. Dam sedimentation reduces its ability to store water and thus limits the dam purpose. Therefore, precise estimations of sediment load are extremely crucial for dam management practices. Several models are proposed to quantify the sediment load, where TerrSet model and RUSLE equations are proven effective. This information can help dam operators decide on regular maintenance, rehabilitation, and sediment management measures and assess the effects of land-use changes such as deforestation and urbanization on soil erosion and sedimentation. Dam managers can increase efficiency and sustainability by assessing the sediment loads using proposed models.

Overall, dam performance and longevity depend on sediment and dam management interactions. Dam sedimentation reduces water storage and availability. Thus, sediment quantification and dam management influence are crucial. TerrSet models can provide accurate and detailed information on entering the dam, which is vital. This information can help dam operators decide on regular maintenance, rehabilitation, and sediment management measures and assess the effects of land-use changes such as deforestation and urbanization on soil erosion and sedimentation. Dam managers can increase efficiency and water resource sustainability by assessing silt-using models.

6. Conclusions

This study analyzed the soil erosion potential zones in the Wadi Baysh using empirical soil erosion model RUSLE integrated with remote sensing, GIS, and TerrSet models. The current research used ALOS PALSAR DEM for basin delineation, which is used as input in the TerrSet model. CHIRPS rainfall data from 2015 to 2020 at an annual scale were used to calculate the R factor in the study area. DSMW and sentinel-2 datasets are acquired to calculate the K factor and LULC classification of the Wadi Baysh, respectively. The significant findings of the study are listed below.

1. R factor calculated using CHIRPS data was found very high in the mountainous regions, which showed a decreasing trend towards the steep slope of the study region. The distribution of R factor demonstrated that Wadi Baysh is extremely vulnerable to soil erosion, especially the northern areas of the basin. Overall, the average values of R factor range from 91.35 to 115.95 MJ mm/ha/h/year in the study area.
2. DSMW is used to calculate the K factor demonstrating the amount of eroded soil and the results revealed low to moderate soil erodibility. Since most of the study area is barren land (81%, estimated using the SVM algorithm), the K factor illustrated high

potential of soil erosion as 58.9% and 75% of the area is comprised of sand in two types of soil classes, respectively.

3. The study area is classified into four major LULC classes, i.e., barren land, built-up, vegetation, and waterbodies. The study area comprises 81%, 11%, 8%, and 1% of barren land, vegetation, and water bodies, respectively.
4. The sediment retention map generated using the TerrSet model after transferring all the input data from the GIS environment showed a total sediment loss of 57.91 million tons at an annual scale. The mountainous regions in Wadi Baysh depicted high risk for soil erosion (with a magnitude of 57.91 tons/ha/year), which is decreasing towards the plan and urban areas.
5. Significant variations in soil loss are observed in the study area, which is associated with topography, agricultural practices, LULC, climate change, and erratic rainfall nature.

Based on these findings, we suggest that this type of sediment will fill the dam's reservoir very soon and, therefore, must be removed or diverted so that it does not reach the dam's reservoir. With this sediment load, the dam will eventually stop functioning if no maintenance is performed.

Author Contributions: Conceptualization, M.E. and J.B.; methodology, J.B., L.Z. and K.U.R.; software, N.E.; validation, N.E., M.E. and J.B.; formal analysis, N.E. and K.U.R.; investigation, N.E. and L.Z.; resources, N.E. and M.E.; data curation, N.E.; writing—original draft preparation, N.E., M.E. and K.U.R.; writing—review and editing, J.B. and H.F.G.; visualization, N.E. and K.U.R.; supervision, J.B. and K.U.R.; project administration, J.B. and H.F.G. All authors have read and agreed to the published version of the manuscript.

Funding: This research received no external funding.

Institutional Review Board Statement: Not applicable.

Informed Consent Statement: Not applicable.

Data Availability Statement: Data used in this study is publicly and freely available, which can be downloaded from the links given in the manuscript.

Acknowledgments: The authors acknowledge the developers of remote sensing and satellite products used in this study, which helped us to carry out the research smoothly.

Conflicts of Interest: The authors declare no conflict of interest.

References

1. Sundara Kumar, P.; Praveen, T.V.; Prasad, M.A.; Rao, P.S. Identification of critical erosion prone areas and computation of sediment yield using remote sensing and GIS: a case study on Sarada river basin. *J. Inst. Eng. Ser. A* **2018**, *99*, 719–728. [CrossRef]
2. Yadav, A.; Satyannarayana, P. Multi-objective genetic algorithm optimization of artificial neural network for estimating suspended sediment yield in Mahanadi River basin, India. *Int. J. River Basin Manag.* **2020**, *18*, 207–215. [CrossRef]
3. Chuenchum, P.; Xu, M.; Tang, W. Estimation of soil erosion and sediment yield in the Lancang–Mekong river using the modified revised universal soil loss equation and GIS techniques. *Water* **2019**, *12*, 135. [CrossRef]
4. Walling, D.E. Measuring sediment yield from river basins. In *Soil Erosion Research Methods*; Routledge: Abingdon, UK, 2017; pp. 39–82.
5. Pande, C.B.; Pande, C. *Sustainable Watershed Development Planning*; Springer: Berlin/Heidelberg, Germany, 2020.
6. Jakubínský, J.; Pechanec, V.; Procházka, J.; Cudlín, P. Modelling of soil erosion and accumulation in an agricultural landscape—A comparison of selected approaches applied at the small stream basin level in the Czech Republic. *Water* **2019**, *11*, 404. [CrossRef]
7. Tamene, L.; Park, S.; Dikau, R.; Vlek, P. Analysis of factors determining sediment yield variability in the highlands of northern Ethiopia. *Geomorphology* **2006**, *76*, 76–91. [CrossRef]
8. Pimentel, D. Soil erosion: a food and environmental threat. *Environ. Dev. Sustain.* **2006**, *8*, 119–137. [CrossRef]
9. Lal, R. Soil Erosion by wind and water: problems and prospects. In *Soil Erosion Research Methods*; RoutledgE: Abingdon, UK, 2017; pp. 1–10.
10. Gisladottir, G.; Stocking, M. Land degradation control and its global environmental benefits. *Land Degrad. Dev.* **2005**, *16*, 99–112. [CrossRef]
11. Bensekhria, A.; Bouhata, R. Assessment and Mapping Soil Water Erosion Using RUSLE Approach and GIS Tools: Case of Oued el-Hai Watershed, Aurès West, Northeastern of Algeria. *ISPRS Int. J. Geo-Inf.* **2022**, *11*, 84. [CrossRef]
12. Les Sols, S. Exploiter Le Potentiel D'adaptation Du Carbone Organique Des Sols Au Changement Climatique. Available online: https://www.fao.org/3/i7268fr/I7268FR.pdf (accessed on 27 March 2022).

13. Singh, G.; Panda, R. Grid-cell based assessment of soil erosion potential for identification of critical erosion prone areas using USLE, GIS and remote sensing: A case study in the Kapgari watershed, India. *Int. Soil Water Conserv. Res.* **2017**, *5*, 202–211. [CrossRef]
14. Belnap, J.; Munson, S.; Field, J. Aeolian and fluvial processes in dryland regions: the need for integrated studies. *Ecohydrology* **2011**, *4*, 615–622. [CrossRef]
15. Walker, B.; Steffen, W. An overview of the implications of global change for natural and managed terrestrial ecosystems. *Conserv. Ecol.* **1997**, *1*, 1662. [CrossRef]
16. Ashiagbor, G.; Forkuo, E.; Laari, P.; Aabeyir, R. Modeling soil erosion using RUSLE and GIS tools. *Int. J. Remote Sens. Geosci.* **2013**, *2*, 1–17.
17. FAO, I. Global Soil Status, Processes and Trends. In *Status of the World's Soil Resources (SWSR)–Main Report*; Food and Agriculture Organization of the United Nations and Intergovernmental Technical Panel on Soils: Rome, Italy, 2015.
18. Diyabalanage, S.; Samarakoon, K.; Adikari, S.; Hewawasam, T. Impact of soil and water conservation measures on soil erosion rate and sediment yields in a tropical watershed in the Central Highlands of Sri Lanka. *Appl. Geogr.* **2017**, *79*, 103–114. [CrossRef]
19. Yeshaneh, G.T. Assessment of soil fertility variation in different land uses and management practices in maybar watershed, South Wollo Zone, North Ethiopia. *Int. J. Environ. Bioremedi. Biodegrad* **2015**, *3*, 15–22.
20. Bahrawi, J.A.; Elhag, M.; Aldhebiani, A.; Galal, H.; Hegazy, A.; Alghailani, E. Soil erosion estimation using remote sensing techniques in Wadi Yalamlam Basin, Saudi Arabia. *Adv. Mater. Sci. Eng.* **2016**, *2016*, 9585962. [CrossRef]
21. García-Ruiz, J.M.; Beguería, S.; Lana-Renault, N.; Nadal-Romero, E.; Cerdà, A. Ongoing and emerging questions in water erosion studies. *Land Degrad. Dev.* **2017**, *28*, 5–21. [CrossRef]
22. Issaka, S.; Ashraf, M. Impact of soil erosion and degradation on water quality: a review. *Geol. Ecol. Landsc.* **2017**, *1*, 1–11. [CrossRef]
23. El Jazouli, A.; Barakat, A.; Ghafiri, A.; El Moutaki, S.; Ettaqy, A.; Khellouk, R. Soil erosion modeled with USLE, GIS, and remote sensing: a case study of Ikkour watershed in Middle Atlas (Morocco). *Geosci. Lett.* **2017**, *4*, 1–12. [CrossRef]
24. Vaezi, A.R.; Abbasi, M.; Keesstra, S.; Cerdà, A. Assessment of soil particle erodibility and sediment trapping using check dams in small semi-arid catchments. *Catena* **2017**, *157*, 227–240. [CrossRef]
25. Montgomery, D.R. Soil erosion and agricultural sustainability. *Proc. Natl. Acad. Sci.* **2007**, *104*, 13268–13272. [CrossRef]
26. Borrelli, P.; Robinson, D.; Panagos, P.; Lugato, E.; Yang, J.; Alewell, C.; Wuepper, D.; Montanarella, L.; Ballabio, C. Land use and climate change impacts on global soil erosion by water (2015–2070). *Proc. Natl. Acad. Sci. USA* **2020**, *117*, 21994–22001. [CrossRef] [PubMed]
27. De Jong, S.; Paracchini, M.; Bertolo, F.; Folving, S.; Megier, J.; De Roo, A. Regional assessment of soil erosion using the distributed model SEMMED and remotely sensed data. *Catena* **1999**, *37*, 291–308. [CrossRef]
28. Boardman, J. Soil erosion science: Reflections on the limitations of current approaches. *Catena* **2006**, *68*, 73–86. [CrossRef]
29. Neitsch, S.L.; Arnold, J.; Kiniry, J.; Williams, J. *Soil and Water Assessment Tool Theoretical Documentation Version 2009*; Texas Water Resources Institute: College Station, TX, USA, 2011.
30. Mitasova, H.; Hofierka, J.; Zlocha, M.; Iverson, L. Modelling topographic potential for erosion and deposition using GIS. *Int. J. Geogr. Inf. Syst.* **1996**, *10*, 629–641. [CrossRef]
31. Natural Capital Project. Available online: https://naturalcapitalproject.stanford.edu/ (accessed on 27 March 2022).
32. CLARKS LABS. Available online: https://clarklabs.org/about/ (accessed on 27 March 2022).
33. Aslam, B.; Khalil, U.; Saleem, M.; Maqsoom, A.; Khan, E. Effect of multiple climate change scenarios and predicted land-cover on soil erosion: A way forward for the better land management. *Environ. Monit. Assess.* **2021**, *193*, 1–25. [CrossRef]
34. El Jazouli, A.; Barakat, A.; Khellouk, R.; Rais, J.; El Baghdadi, M. Remote sensing and GIS techniques for prediction of land use land cover change effects on soil erosion in the high basin of the Oum Er Rbia River (Morocco). *Remote Sens. Appl. Soc. Environ.* **2019**, *13*, 361–374. [CrossRef]
35. Masoud, M.H.; Basahi, J.; Zaidi, F. Groundwater resource management based on three-dimensional flow modeling of Wadi Baysh aquifer system: southwestern Saudi Arabia. *Environ. Earth Sci.* **2019**, *78*, 1–18. [CrossRef]
36. Abu-Abdullah, M.M.; Youssef, A.; Maerz, N.; Abu-AlFadail, E.; Al-Harbi, H.; Al-Saadi, N. A flood risk management program of Wadi Baysh dam on the downstream area: An integration of hydrologic and hydraulic models, Jizan region, KSA. *Sustainability* **2020**, *12*, 1069. [CrossRef]
37. ASF. Available online: https://search.asf.alaska.edu/#/ (accessed on 27 March 2022).
38. Funk, C.; Peterson, P.; Landsfeld, M.; Pedreros, D.; Verdin, J.; Shukla, S.; Husak, G.; Rowland, J.; Harrison, L.; Hoell, A. The climate hazards infrared precipitation with stations—a new environmental record for monitoring extremes. *Sci. Data* **2015**, *2*, 1–21. [CrossRef]
39. Sousa, K.D.; Sparks, A.; Ashmall, W.; Etten, J.; Solberg, S. chirps: API Client for the CHIRPS Precipitation Data in R. *J. Open Source Softw.* **2020**. [CrossRef]
40. Shahid, M.; Rahman, K.; Haider, S.; Gabriel, H.; Khan, A.; Pham, Q.; Mohammadi, B.; Linh, N.; Anh, D. Assessing the potential and hydrological usefulness of the CHIRPS precipitation dataset over a complex topography in Pakistan. *Hydrol. Sci. J.* **2021**, *66*, 1664–1684. [CrossRef]
41. Food and Agriculture Organization of United Nations. Available online: https://www.fao.org/soils-portal/data-hub/soil-maps-and-databases/en/ (accessed on 27 March 2022).
42. United Nation Geological Survey Earth Explorer. Available online: https://earthexplorer.usgs.gov/ (accessed on 27 March 2022).
43. Helder, D.; Markham, B.; Morfitt, R.; Storey, J.; Barsi, J.; Gascon, F.; Clerc, S.; LaFrance, B.; Masek, J.; Roy, D. Observations and recommendations for the calibration of Landsat 8 OLI and Sentinel 2 MSI for improved data interoperability. *Remote Sens.* **2018**, *10*, 1340. [CrossRef]

44. eoPortal. Available online: https://www.eoportal.org/satellite-missions/copernicus-sentinel-2#performance-specifications (accessed on 27 March 2022).
45. Chuenchum, P.; Xu, M.; Tang, W. Predicted trends of soil erosion and sediment yield from future land use and climate change scenarios in the Lancang–Mekong River by using the modified RUSLE model. *Int. Soil Water Conserv. Res.* **2020**, *8*, 213–227. [CrossRef]
46. Kenneth, G.R.; George, R.; Glenn, A.; Jeffrey, P. RUSLE: Revised universal soil loss equation. *J. Soil Water Conserv.* **1991**, *46*, 30–33.
47. Tsegaye, L.; Bharti, R. Soil erosion and sediment yield assessment using RUSLE and GIS-based approach in Anjeb watershed, Northwest Ethiopia. *SN Appl. Sci.* **2021**, *3*, 1–19. [CrossRef]
48. Maleika, W. Inverse distance weighting method optimization in the process of digital terrain model creation based on data collected from a multibeam echosounder. *Appl. Geomat.* **2020**, *12*, 397–407. [CrossRef]
49. Liu, D.; Zhao, Q.; Fu, D.; Guo, S.; Liu, P.; Zeng, Y. Comparison of spatial interpolation methods for the estimation of precipitation patterns at different time scales to improve the accuracy of discharge simulations. *Hydrol. Res.* **2020**, *51*, 583–601. [CrossRef]
50. Hurni, H. An ecosystem approach to soil conservation. In *Soil Erosion and Conservation*; El-Swaify, S.A., Moldenhauer, W.C., Lo, A., Eds.; Soil Conservation Society of America: Ankey, IA, USA, 1985; pp. 759–771.
51. Singh, M.; Khera, K. Soil erodibility indices under different land uses in lower Shiwaliks. *Trop. Ecol.* **2008**, *49*, 113.
52. Wawer, R.; Nowocien, E.; Podolski, B. Eal and calculated kusle erobility factor for selected Polish soils. *Pol. J. Environ. Stud.* **2005**, *14*, 655–658.
53. Neitsch, S. Theoretical Documentation*Erosion Soil and Water Assessment Tool*; Texas Agricultural Eksperiment Station: Temple, TX, USA, 2000; p. 625.
54. Adugna, T.; Xu, W.; Fan, J. Comparison of random forest and support vector machine classifiers for regional land cover mapping using coarse resolution FY-3C images. *Remote Sens.* **2022**, *14*, 574. [CrossRef]
55. Balkhair, K.S.; Rahman, K.U. Development and assessment of rainwater harvesting suitability map using analytical hierarchy process, GIS and RS techniques. *Geocarto Int.* **2021**, *36*, 421–448. [CrossRef]
56. Motlagh, Z.K.; Lotfi, A.; Pourmanafi, S.; Ahmadizadeh, S.; Soffianian, A. Spatial modeling of land-use change in a rapidly urbanizing landscape in central Iran: Integration of remote sensing, CA-Markov, and landscape metrics. *Environ. Monit. Assess.* **2020**, *192*, 1–19. [CrossRef] [PubMed]
57. Parida, B.R.; Mandal, S. Polarimetric decomposition methods for LULC mapping using ALOS L-band PolSAR data in Western parts of Mizoram, Northeast India. *SN Appl. Sci.* **2020**, *2*, 1–15. [CrossRef]
58. Daba, M.H.; You, S. Quantitatively assessing the future land-use/land-cover changes and their driving factors in the upper stream of the Awash River based on the CA–markov model and their implications for water resources management. *Sustainability* **2022**, *14*, 1538. [CrossRef]
59. Jensen, J.R. *Introductory Digital Image Processing: A Remote Sensing Perspective*; Prentice-Hall Inc.: Hoboken, NJ, USA, 1996.
60. Congalton, R.G. A review of assessing the accuracy of classifications of remotely sensed data. *Remote Sens. Environ.* **1991**, *37*, 35–46. [CrossRef]
61. Maqsoom, A.; Aslam, B.; Hassan, U.; Kazmi, Z.; Sodangi, M.; Tufail, R.; Farooq, D. Geospatial assessment of soil erosion intensity and sediment yield using the revised universal soil loss equation (RUSLE) model. *ISPRS Int. J. Geo-Inf.* **2020**, *9*, 356. [CrossRef]
62. Saleem, U.; Amjad, A.; Muhammad, I.; Muhammad, J.; Muhammad, I. Geospatial assessment of soil erosion intensity and sediment yield: a case study of Potohar Region, Pakistan. *Environmental Earth Sciences* **2018**, *77*, 1–13.
63. Obaid, H.; Shahid, S. Soil erosion susceptibility of Johor River basin. *Water Environ. J.* **2017**, *31*, 367–374. [CrossRef]
64. Tadesse, L.; Suryabhagavan, K.; Sridhar, G.; Legesse, G. Land use and land cover changes and Soil erosion in Yezat Watershed, North Western Ethiopia. *Int. Soil Water Conserv. Res.* **2017**, *5*, 85–94. [CrossRef]
65. Azaiez, N.; Alleoua, A.; Baazaoui, N.; Qhtani, N. Assessment of soil loss in the Mirabah Basin: an overview of the potential of agricultural terraces as ancestral practices (Saudi Arabia). *Open J. Soil Sci.* **2020**, *10*, 159. [CrossRef]
66. Elhag, M.; Hidayatulloh, A.; Bahrawi, J.; Chaabani, A.; Budiman, J. Using inconsistencies of wadi morphometric parameters to understand patterns of soil erosion. *Arab. J. Geosci.* **2022**, *15*, 1–14. [CrossRef]
67. Moses, A. GIS-RUSLE interphase modelling of soil erosion hazard and estimation of sediment yield for river Nzoia basin in Kenya. *J Remote Sens GIS* **2017**, *6*, 1–13. [CrossRef]
68. Xu, L.; Xu, X.; Meng, X. Risk assessment of soil erosion in different rainfall scenarios by RUSLE model coupled with Information Diffusion Model: A case study of Bohai Rim, China. *Catena* **2013**, *100*, 74–82. [CrossRef]
69. Azaiez, N.; Baazaoui, N.; Blel, I.; Hammami, B. Contribution of the adjusted empirical analysis of the RSULE and FAO models in the estimation of soil losses in the watershed of Wadi El Hayat (Saudi Arabia). *Arab. J. Geosci.* **2021**, *14*, 1–18. [CrossRef]
70. Wolka, K.; Tadesse, H.; Garedew, E.; Yimer, F. Soil erosion risk assessment in the Chaleleka wetland watershed, Central Rift Valley of Ethiopia. *Environ. Syst. Res.* **2015**, *4*, 1–12. [CrossRef]
71. Tirkey, A.S.; Pandey, A.; Nathawat, M. Use of satellite data, GIS and RUSLE for estimation of average annual soil loss in Daltonganj watershed of Jharkhand (India). *J. Remote Sens. Technol.* **2013**, *1*, 20–30. [CrossRef]

Disclaimer/Publisher's Note: The statements, opinions and data contained in all publications are solely those of the individual author(s) and contributor(s) and not of MDPI and/or the editor(s). MDPI and/or the editor(s) disclaim responsibility for any injury to people or property resulting from any ideas, methods, instructions or products referred to in the content.